PHYSICAL REVIEW D VOLUME 25, NUMBER 5 1 MARCH 1982

Study of charge-dependent behavior of final-state particles in $\pi^- p$ interactions at 205 GeV/c

G. P. Yost, H. H. Bingham, D. M. Chew,* B. Y. Daugeras,† W. B. Fretter, W. R. Graves,‡ J. -F. Grivaz†, A. D. Johnson, J. A. Kadyk, L. Stutte,§ and F. C. Winkelmann
Department of Physics and Lawrence Berkeley Laboratory, University of California, Berkeley, California 94720

D. Bogert, R. Hanft, R. Harris,|| S. Kahn,¶ C. Pascaud,† and W. M. Smart
Fermi National Accelerator Laboratory, Batavia, Illinois 60510
(Received 23 February 1979; revised manuscript received 30 September 1981)

Inelastic channels in $\pi^- p$ interactions at 205 GeV/c are studied as a function of charged-particle multiplicity n_{ch}. Experimental tests are made which are sensitive to the charge-dependent behavior of the particles, particularly at high and low rapidities. A set of new variables useful for the study of these processes is introduced. Effects which may be attributed to leading particles or leading jets are present to some extent for all n_{ch}. Among the results presented, it is shown that at this energy there is no "central region" which is completely free of effects which are correlated with the charges of the incident particles. Qualitative interpretation of the results in terms of cluster-model ideas is presented; a specific simple model is calculated and compared with the data.

I. INTRODUCTION

We report on an investigation of the inelastic channels in $\pi^- p$ interactions at 205 GeV. Many recent analyses of similar reactions concentrate on the characteristics of the "central region," i.e., that kinematic region containing those particles emitted with momenta near zero in the center of mass. In this paper, we present results which are most sensitive to the characteristics of what we shall call the "extreme" region, roughly complementary to the central region, consisting of those particles with relatively large forward or backward center-of-mass (c.m.) momenta. These particles predominantly carry the beam or target charge, respectively, as is well known on an inclusive basis[1] from Feynman-x and rapidity studies.

We study this from novel points of view, as a function of charged-particle multiplicity, in both c.m. and laboratory systems. We include the neutral particles, taken as a system, and uncover some interesting behavior. For example, on an event-by-event basis, the neutrals' system is as strongly forward-backward asymmetric (in the c.m.) as either the negatives' system or positives' system. However, the sign of the asymmetry for the neutrals' system varies, so that if one averages over all events, the asymmetry approximately vanishes.

We observe what can perhaps be best described as systems (e.g., jets or clusters) carrying a net charge. These subsequently decay into several final-state particles in such a manner that most of the momentum of the system may, with a certain probability, be carried away by particles of any given charge. We present data and analyses which provide new tests of detailed models of production. We show a comparison with one such model.

In Sec. II we present a brief review of experimental details. The results are given in Sec. III, beginning with a discussion in terms of momentum and energy variables. We then analyze in some detail the charge structure of these regions, using the rapidity variables, measured with respect to the most extreme (highest or lowest rapidity) charged particle. In Sec. IV, there is a brief comparison with a specific cluster model. A summary of the results is given in Sec. V. An appendix discusses experimental corrections. A description of the experiment and some of its other results appear elsewhere.[2–9]

II. EXPERIMENTAL DETAILS

General

The data come from a 48 000-picture exposure of the Fermilab hydrogen-filled 30-inch bubble

chamber to a 205±1 GeV negative beam (Fermilab experiment number E137). The beam contained 95.8% π^-, contaminated with 2.6% μ^-, 1.4% K^-, and 0.2% $\bar{p}$. The results to be presented are not sensitive to beam contamination.

In order to improve the momentum and angle measurement precision, the event sample is restricted to a fiducial volume such that forward-going tracks have a potential length of at least 30 cm.

The events were measured on film-plane digitizers with a root-mean-square scatter of measured points about the reconstruction track (FRMS) of less than two microns on film. View-by-view track matching was done by eye. The measuring precision was sufficiently great that most errors in matching were detectable by the value of FRMS. Spatial track reconstruction to find curvature (and hence, momentum) and angles was done with TVGP[10]; kinematic fitting, where used (to identify channels with no missing neutrals), was done with SQUAW.[10] All tracks were required to satisfy certain goodness-of-reconstruction criteria in TVGP, including a sign of curvature in agreement with that deduced from charge conservation; otherwise the event was remeasured at least once (some up to four times).[4]

The elastic-scattering channel, identified on the basis of kinematic fits,[3] was removed from the sample. A relative weight is applied to each successfully measured event to compensate for topology-dependent differences in the fraction of the film measured and in scanning and measuring efficiences.[4] The number of events and the relative weight of each topology (normalized to the two-pronged events) are given in Table I. These weights are based on the cross sections given in Ref. 9, and assume that the only biases which occur in the losses are those which depend on the topology. The average number of charged secondaries[9] is $\langle n_{ch} \rangle = 7.99 \pm 0.06$, the total elastic cross section is 3.18 mb, and the total inelastic cross section is 21.00 mb.

An estimated[3] 20 misidentified elastic events contaminate the two-prong sample; an estimated 8 inelastic events are incorrectly identified as elastic and removed. No corrections are made for these small effects.

Track identification

All tracks are assumed to be pions unless identified as protons by the scanners or the reconstruction (see the Appendix). From the momentum spectrum of identified protons, we infer that the fraction of protons within the momentum range for efficient identification decreases as n_{ch} increases. We have therefore computed a weighting factor as an average correction, as described in the Appendix, for the underestimation of the laboratory energy of the positive tracks due to misidentification of a proton as a pion. This correction, nor-

TABLE I. Raw numbers of events and relative weights.

n_{ch}	No. events	Relative weight[a]
2	202[b]	1.00
4	381	1.11
6	405	1.17
8	390	1.28
10	207	1.94
12	129	2.06
14	53	2.54
16	37	2.01
18[c]	11	3.39
Total	1815	
	$\langle n_{ch} \rangle = 7.99 \pm 0.06$	

[a]Based on cross sections of Ref. 9; see text for explanation.

[b]Inelastic only.

[c]There are five events with $n_{ch} \geq 20$, which are found to have no signifcant effects on the conclusions of the paper; they have been neglected throughout.

mally small in comparison with the structure in the data, has been applied to all data presented. We find that low-multiplicity events are largely unaffected; high-multiplicity data require a correction in some variables. Data for neutral-particle production, estimated from charged-particle data using conservation of energy and momentum, have been likewise corrected. No allowance for possible systematic errors in the correction is included in quoted errors. We emphasize that the measured behavior of negative tracks is unaffected by proton misidentification, and that laboratory-system momenta are unaffected for any sign of charge.

It is estimated from visible K^0 decays and γ conversions[9] that 4% of all secondary tracks are K^+ or K^-, and an additional 1% are e^+ or e^- resulting from Dalitz decays; the rate of $\bar{p}$ production is expected to be even smaller. No correction has been computed for these small effects.

Momentum biases

The bubble-chamber technique yields unbiased measurements of the curvature k of tracks in the magnetic field,[10] from which the momentum component perpendicular to the field may be derived, given by α/k, α a constant. For a large number of measurements performed on a given track, k will be randomly distributed approximately as a Gaussian; hence the distribution of p will be asymmetric, with a bias such that the mean value $\langle p \rangle$ is larger than $\alpha/\langle k \rangle$. After detailed analysis, we have concluded that this bias is reduced to a level which is unimportant within our statistical errors if we impose the constraint that no event which contains a track whose measured momentum exceeds 400 GeV/c (twice the physical limit) is accepted into the final sample. As previously discussed, the cutoff on wrong-sign measured curvature is also imposed. The weights in Table I include corrections for these cuts.

Other biases can result from imperfect correction for optical distortions.[4] To check for this type of effect, the entire event sample has been reconstructed with each of two independently determined sets of optical corrections. The only appreciable difference occurs for $n_{\rm ch}=2$, of magnitude about one standard deviation in some variables.

There is no significant evidence of a difference between momentum "pull" quantities for positive and negative tracks, either for events which have a four-constraint (4C) fit, or the V^0's which have a 3C K^0 or Λ fit. We therefore conclude that there is no reason to expect that differences between positive and negative tracks arise from measurement biases.

The final outcome of our procedures was tested by looking at events identified (by kinematic fits) as elastic scattering. Here the outgoing π^-, with very nearly the full energy of the beam, has the largest momentum errors likely to be encountered. We find the mean measured momentum of the elastically scattered π^- to be 201.8 ± 4.6 GeV/c, with the present selections. We believe therefore that it is unlikely that our procedures have resulted in any important net bias of the measured momenta.

III. ANALYSIS AND RESULTS

A. Momentum and energy variables

The observation from inclusive studies that particles of beamlike charge tend to go forward and particles of targetlike charge tend to go backward in the c.m. has been attributed frequently in the literature to the phenomenon of "leading particles."[11] A leading "particle" may be thought of as that particle or collection of particles which may be identified in some way (perhaps only theoretically) as fragments of the beam or target. It is frequently supposed that these fragments carry the quantum numbers (in particular, the charge) of the fragmenting particle most of the time.[12] In QCD these particles may take the form of jets of fragmenting quarks. In a four-jet model, the struck quarks and the spectator quarks each form jets. If the four-momentum transferred to the struck quark is somehow damped, then its fragments carry a significantly larger fraction of the beam or target c.m. momentum than expected from phase space, hence leading particles are formed. The products of beam or target diffractive dissociations form a particularly clear example of this behavior. We shall show that, for all multiplicities, it is a poor description of the data to assume that leading particles are predominantly composed of a single particle of a particular charge.

We specialize to a set of variables sensitive to the distribution of final-state particles in the most forward and backward kinematic regions in the c.m. We hope thereby to achieve enhanced sensitivity to the nature of the direct coupling of beam and target with the exchange mechanism(s) responsible for the reaction. We make no attempt to

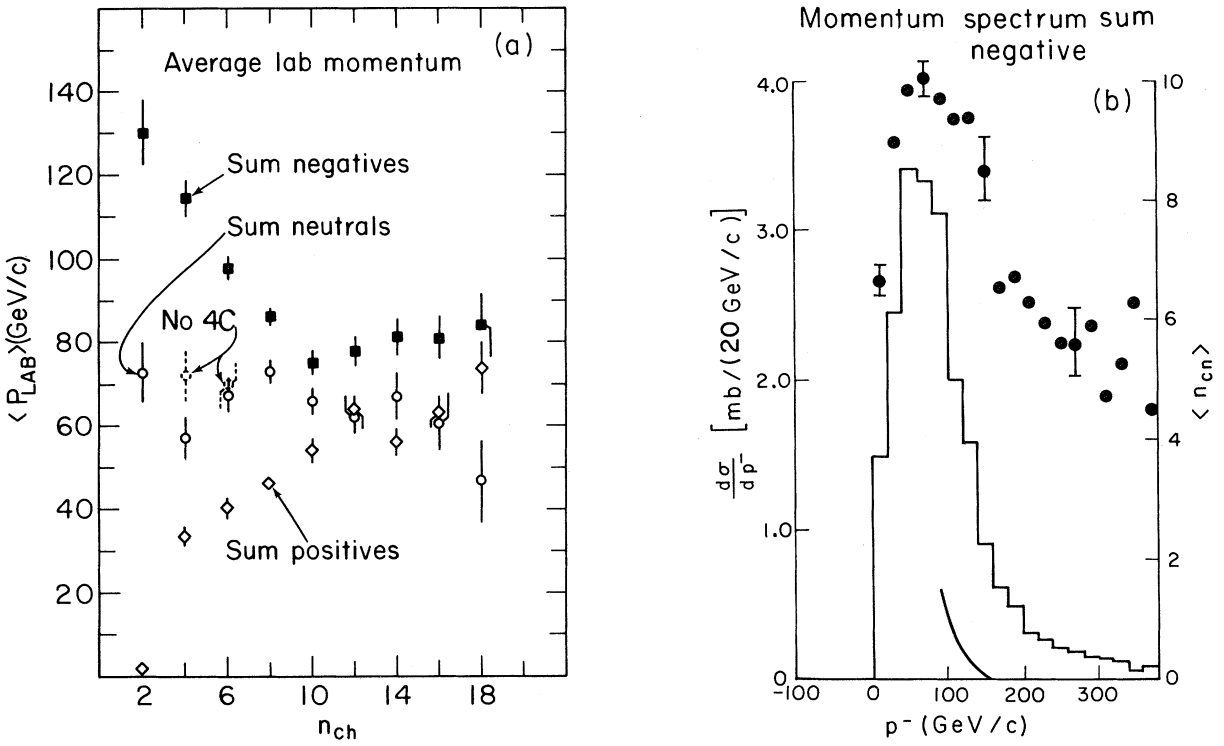

FIG. 1. (a) Average laboratory momentum of vector sum of negative tracks (solid squares) and of positive tracks (open diamonds). The average missing momentum is also shown (open circles). Dashed open circles show same after removal of events with no neutrals. The same convention relating type of symbol and particle charge will be maintained throughout; (b), (c), and (d) Bar graph and left-hand scale: laboratory momentum distribution for vector sum of negative, positive, and neutral tracks, respectively. Scale is in mb/20 GeV/c. Charged momenta >205 and neutral (missing) momenta <0 GeV/c occur as a result of measurement error. Points (some with errors) and right-hand scale: average charged-particle multiplicity. Solid curves in Figs. 1(b) and 1(c) are estimated background in region shown due to mismeasurement of lower momenta (see text).

separate or identify individual leading particles, e.g., on the basis of large rapidity gaps.

Laboratory frame

First, we study the laboratory charged-summed momentum: for events of a given multiplicity ("multiplicity" refers to charged-particle multiplicity n_{ch} throughout) we evaluate the laboratory-momentum magnitude of the system composed of all particles of a given charge. Since most neutral particles are not seen in the bubble chamber, we evaluate their momenta by subtraction.

Formally,

$$p^c_{\rm lab} = \left| \sum_{i=1}^{n_j^c} \vec{p}^{\,i}_{\rm lab} \right| , \tag{1}$$

where n_j^c is the number of particles of charge c in event j, and $\vec{p}^{\,i}_{lab}$ is the laboratory-momentum vector of particle i. We find $p^0_{\rm lab}$ by

$$p^0_{\rm lab} = p^{\rm beam}_{\rm lab} - \left| \vec{p}^{\,+}_{\rm lab} + \vec{p}^{\,-}_{\rm lab} \right|_{\rm long} , \tag{2}$$

which neglects the transverse momentum of the neutrals, for simplicity. Using this procedure we can treat neutral particles formally in the same manner as charged particles. Because they are evaluated in the laboratory frame these quantities are virtually independent of track mass assignment. In what follows, we drop the subscript "lab" for convenience.

We give the average p^c in Fig. 1(a) as a function of n_{ch}. We observe that the negative tracks carry significantly greater momentum than either neutrals or positives, for all n_{ch}. The negatives and positives converge rapidly toward each other until $n_{ch} \cong 10$, but these momentum sums are approximately flat with n_{ch} thereafter.

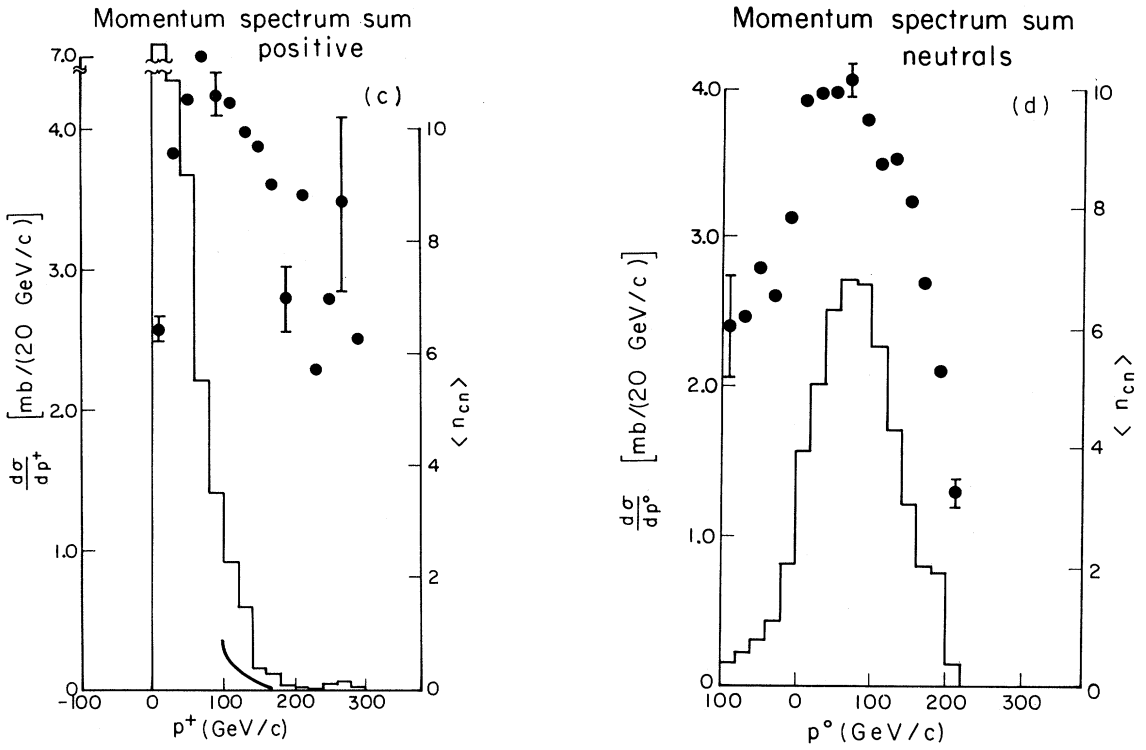

FIG. 1. (*Continued.*)

The neutral particles, which are about equal in numbers,[9] on the average, with the positives or negatives over this n_{ch} range, behave as the average of negatives and positives, sharing roughly $\frac{1}{3}$ the available laboratory momentum independent (approximately) of n_{ch} up to $n_{ch} \cong 14$. The dip in p^0_{lab} at $n_{ch}=4$ may be attributed to the existence of events with no neutral particles (such events for $n_{ch}=2$, i.e., elastic scattering, have already been removed; for $n_{ch} \geq 6$ they comprise a negligible fraction of the channels). We identify these events by 4C fits. When they are removed (dashed points), the dip disappears.

Momentum distribution in the laboratory

In Figs. 1(b)—1(d) we show the inclusive distribution $d\sigma/dp^c$ separately for negative, positive, and neutral charges. We also show $\langle n_{ch} \rangle$ as a function of p^c (solid points). The distribution of negative p^c shows a peak at about 80 GeV/c with a long tail extending to high energies, as expected for negative leading particles. More remarkable is the distribution of positives, which shows that about 9% of the cross section has positive particles which sum to momenta ≥ 100 GeV/c, indicating that more than half of the total momentum was transferred from the negative beam to positive particles.

Errors in measurement at these high-momenta contribute to both the p^+ and p^- high-energy tails. An estimate of the low-momentum contribution to the $p^{\pm} \geq 100$ GeV/c region, determined from Gaussian ideograms in $1/p^{\pm}$, is shown in the solid curves in Figs. 1(b) and 1(c). Losses *out* of the region $100 \leq p^{\pm} \leq 400$ GeV/c approximately compensate. We find that the total cross section for $p^+ > 100$ GeV/c is 1.9 mb, or 9% of the total inelastic cross section. This may be compared with 6.5 mb (31%) for $p^- \geq 100$ GeV/c, corrected in the same way for measurement error.

We conclude that this is not an artifact of experimental resolution, because the large-p^+ events have indeed very low p^-: $\langle p^+ - p^- \rangle$ for the $p^+ \geq 100$ GeV/c sample is 86 ± 5 GeV/c, compared with -49 ± 2 GeV/c for the full data, and $\langle p^- \rangle = 57 \pm 2$ GeV/c compared with 93 ± 2 GeV/c for all events. Therefore in an appreciable number of events, the usual leading-particle picture of beam fragments carrying the same net charge and most of the momentum of the beam particle is invalid.

One might naively expect that events with large

p^+ would be dominated by high multiplicities, in which large amounts of the beam energy are expended in particle creation. This would leave less energy to distinguish leading particles from other particles [see e.g., Fig. 1(a)] and hence, perhaps, an enhanced likelihood that a fluctuation would cause a number of positive particles together to carry off a large amount of energy. However, the average $n_{\rm ch}$ dips sharply for large p^+ [Fig. 1(c)], in disagreement with this picture. This latter result cannot be predicted on the basis of Fig. 1(a) alone, where there is evidence that the *low*-multiplicity events possess particularly large p^- and small p^+.

Figure 1(d) shows the momentum spectrum of the neutrals, Eq. (2). Since large p^0 comes from events with simultaneously small p^+ and p^-, it is a region of high measurement accuracy (as evidence for which, we point out the absence of a tail of events beyond 205 GeV/c), so we make no corrections of the type made for p^+ and p^- above. About 33% of the cross section for p^0 lies above 100 GeV/c, approximately equal to the fraction with $p^- > 100$ GeV/c. About 10% lies above 160 GeV/c, which is 80% of the beam momentum. Clearly, large missing momentum is as important as large negative momentum in the final states of these reactions.

As for the positives and negatives, large missing momenta (high values of p^0) are dominated by events with few charged particles. This suggests that the dynamical mechanism responsible for producing very large p^c may be similar for all charges c, differing only in intenisty. The average multiplicity of events containing neutral particles of momenta larger than 100 GeV/c is 4.8, well below the overall average multiplicity (7.99). However, even in events with many charged particles, more than half the available momentum is often found to be carried by neutral particles: e.g., 20% of the 14-pronged events and 13% of the 16-pronged events have $p^0 \geq 100$ GeV/c.

Finally, comparing the behavior of the average charged-particle multiplicity as a function of p^-, p^+, and p^0 [solid points, Fig. 1(b)—1(d)], we observe considerable similarity. This is in contrast with the behavior of the "inverse" distributions, which are the average p^-, p^+, and p^0 as a function of $n_{\rm ch}$, Fig. 1(a).

We conclude from this discussion that the transfer of significant amounts of the beam momentum to particles of charge different from the beam charge is an important process. We shall return to this question subsequently. This effect is most important for low multiplicities. The events with the largest, and also the smallest, values of p^c are dominated by the low multiplicites; high-multiplicity events dominate in the region $p^c \sim \frac{1}{3} p_{\rm beam}$.

Momentum distributions in the center of mass

To study momentum distributions in the c.m. we introduce charge-summed quantities analogous to those we just used. First, we calculate

$$x^c = \sum_{i=1}^{n_j^c} x_i \ , \tag{3}$$

and, second $|x^c|$, where x is the Feynman x ($x = p_{||}^{\rm c.m.}/p_{\rm max}^{\rm c.m.}$). The summations run over all tracks of a given event, as before. In this experiment, $p_{\rm max}^{\rm c.m.} \cong \sqrt{s}/2$, and $\sqrt{s} = 19.65$ GeV. We consider averages over topologies, $\langle x^c \rangle$ and $\langle |x^c| \rangle$.

These variables are useful for (among other things) the following reasons. The sign of x_i varies from track to track, and the sign of $\sum_{i=1}^{n_j^c} x_i$ varies from event to event. When averaging x^c over a topology to obtain $\langle x^c \rangle$, partial cancellations of both the track-by-track and event-by-event types are important. Only the track-by-track cancellations play a role in $\langle |x^c| \rangle$. If event-by-event cancellations are negligible,

$$\langle |x^c| \rangle \cong |\langle x^c \rangle| \ . \tag{4}$$

These observations motivate the use of another variable η^c, the fraction of the total energy ($=\sqrt{s}$) available in the c.m. which is possessed by the system in question[13]:

$$\eta^c = \sum_{i=1}^{n_j^c} \eta_i \ . \tag{5}$$

Energy-momentum conservation requires $\eta \lesssim 0.5$ for any system of mass $<< \sqrt{s}$. The relationship of η^c to x^c and $|x^c|$ is based on the placement of the absolute-value signs:

$$\eta^c \approx \frac{1}{2} \left[\sum_{i=1}^{n_j^c} |x_i| \right] . \tag{5'}$$

This equation is exact in the limit of negligible masses and transverse momenta. Neither event-by-event nor track-by-track cancellations affect $\langle \eta \rangle$ (we will henceforth drop the superscript c).

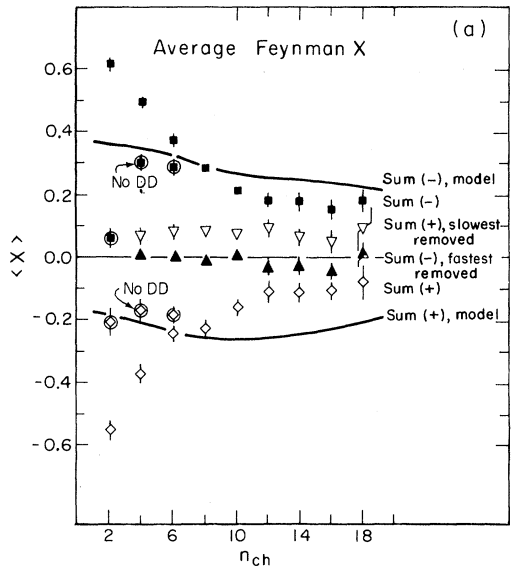

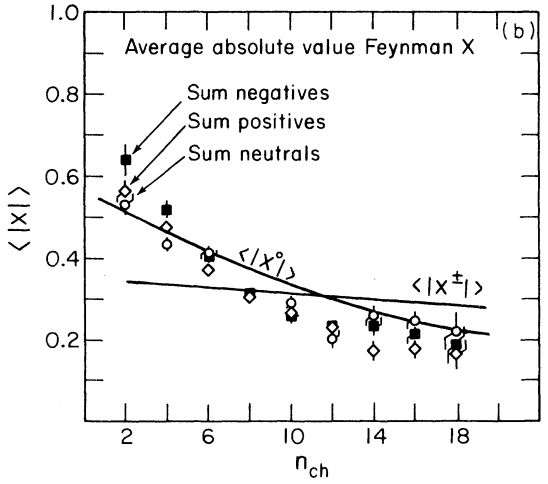

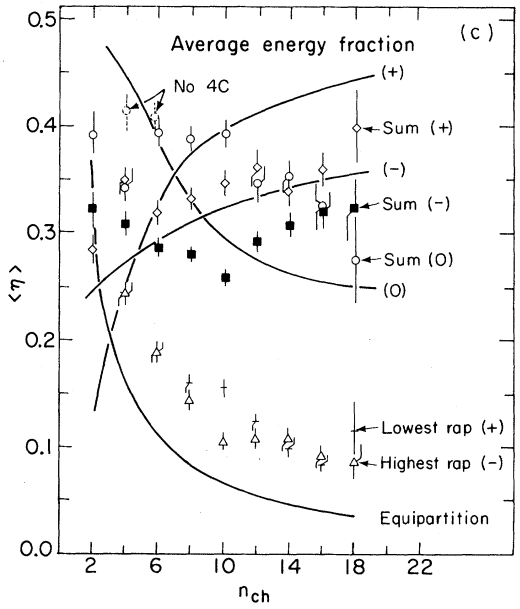

FIG. 2. (a) Average value of $x\,(=p_{\parallel}^{\text{c.m.}}/p_{\max}^{\text{c.m.}})$ as a function of n_{ch} for the sum of all negative tracks (solid squares) and of all positive tracks (open diamonds). Results with diffraction dissociation candidate events (defined in Ref. 14) removed are given by same symbols, circled. Also shown: the same sums but with the highest-(laboratory) momentum negative or the lowest-momentum positive removed (negatives, solid erect triangles; positives, open inverted triangles). Solid curves on this and subsequent figures are model calculation for comparison with full data, to be discussed in Sec. IV. (b) Average absolute value of x for same charge-summed quantities as in part (a). (c) The energy fraction $\eta(=E_{\text{c.m.}}/\sqrt{s})$, averaged over all events of a given topology, for the same charge-summed quantities as in part (a). Also shown: the single highest-rapidity negative (open triangles), and the single lowest-rapidity positive (+ symbols). For comparison, the single-particle average η is shown by the solid line ("equipartition"), assuming equal number of positive, negative, and neutral particles.

Hence, if track-by-track cancellations do not occur, then $\langle \eta \rangle \cong \frac{1}{2}\langle |x| \rangle$. Equation (5′) is experimentally accurate to about 5—10% for low n_{ch}, and 20—30% at high n_{ch}, based on charged particles. We use η rather than the right-hand side of (5′) because the latter cannot be evaluated for neutrals.

Quantities for neutral particles are obtained by subtraction, as before.

The results appear in Fig. 2. The solid curves on this and many subsequent figures represent the results of a model calculation, which will be discussed in Sec. IV.

In Fig. 2(a) we observe that the relative behavior of $\langle x^{\pm} \rangle$ shows the same general structure observed in Fig. 1, namely, rapid approach of $\langle x^{+} \rangle$ and $\langle x^{-} \rangle$ toward each other for low n_{ch}, nearly flat behavior for high n_{ch}. Because of the similarity to the results of Fig. 1, we conclude that the qualitative behavior of $\langle x^{+} \rangle$ and $\langle x^{-} \rangle$ cannot be a result of errors in track mass identification (such errors have negligible effects on Fig. 1).

In order to avoid confusion, the neutrals have not been included on this figure. We compute that $\langle x^{0} \rangle \equiv -(\langle x^{+} \rangle + \langle x^{-} \rangle)$ is roughly independent of n_{ch} and lies in the region -0.05 to -0.10. A possible explanation for the neutrals moving backward in the c.m., on the average, is the effects of production of neutrons or other neutral baryons associated with target fragmentation. Because of their relatively large mass, such particles could more than compensate for forward-going neutral mesons.

The data of Fig. 2(a) suggest the leading-particle behavior described earlier. Interpreted this way, evidence for leading-particle behavior is present (a) equally at beam and target vertices, (b) in all multiplicities, and (c) beyond $n_{ch} = 10$ shows no signs of decreasing to zero as n_{ch} increases.

We also show on Fig. 2(a) the result obtained for $\langle x^{\pm} \rangle$ when the highest-x negative or lowest-x positive particle is excluded from the sum. The simplifying assumption is sometimes made that these single particles may be identified as the leading particles. We find that $\langle x_R^{+} \rangle$ (where R means "residual") actually exceeds $\langle x_R^{-} \rangle$ by a small amount, but both are consistent with n_{ch}-independence and near zero, as would be expected if the leading particles had been removed. Hence we conclude that, in this limited way, the idea of a single-particle leading "particle" has some experimental validity for all topologies. However, evidence given earlier, and to be given below, is not consistent with this definition of a leading particle.

When events identified as proceeding via diffraction dissociation (DD)[14] are removed [encircled points, Fig. 2(a); less than 1% of the events of $n_{ch} \geq 10$ are removed], we observe that the data show significantly less n_{ch} dependence.[15]

In Fig. 2(b) we show $\langle |x^{c}| \rangle$ for the full data where the averaging is, as before, done separately for each n_{ch}. For the neutral particles, $\langle |x^{0}| \rangle$ is about as large as $\langle |x^{\pm}| \rangle$ and as strongly dependent on n_{ch}, in striking contrast with $\langle x^{0} \rangle$, which is small (-0.05 to -0.10) and independent of n_{ch}. It follows, in view of the definitions of $\langle x \rangle$ and $\langle |x| \rangle$, that the event-by-event cancellations in $\sum_{i=1}^{n} x_i$ play an important role for the neutral particles. Thus, on any given event (including the highest multiplicities), the neutral particles are produced with about the same degree of asymmetry (in the c.m.) as the charged particles, but the sign of the asymmetry varies from one event to another, leaving the average of x^{0} over all events small, but the average of $|x^{0}|$ large.

Both $\langle |x^{+}| \rangle$ and $\langle |x^{-}| \rangle$ lie close to their lower limits $|\langle x^{\pm} \rangle|$ indicating that there is little or no event-by-event cancellation affecting $\langle x^{\pm} \rangle$. That is, for most events $\sum x_i^{-}$ is positive (beam direction) and $\sum x_i^{+}$ is negative (target direction).

The behavior of $\langle \eta \rangle$ is shown in Fig. 2(c). Perhaps the most striking difference between the behavior of $\langle \eta \rangle$ and those variables shown previously is that the topology dependences of $\langle \eta^{0} \rangle$, $\langle \eta^{+} \rangle$, and $\langle n^{-} \rangle$ are comparatively weak and qualitatively similar to each other. Almost absent here is the rapid variation at low n_{ch} seen for $\langle x \rangle$ and $\langle |x| \rangle$. In detail, $\langle \eta^{+} \rangle$ is nearly constant (or shows at most a gradual rise). $\langle n^{-} \rangle$ shows a weak n_{ch} dependence, with a change in slope at $n_{ch} = 10$, the approximate location of the onset of the changes in behavior seen in previous figures.

The neutrals have a larger fraction of the c.m. energy than either the positives or the negatives, at least up to $n_{ch} = 10$, beyond which point $\langle \eta^{0} \rangle$ appears to be falling. Since the average number of neutral particles per event is about equal to the number of negative or positive particles,[9] for most n_{ch}, these large neutral c.m. energies are not simply due to the presence of large numbers of neutral particles. This large share of the energy suggests that neutral particles are important participants in any leading-particle formation that occurs at either beam or targe vertex. The large c.m. asymmetries noted earlier suggest that the excess of $\langle \eta^{0} \rangle$ over $\langle n^{\pm} \rangle$ is not, however, due to neutral particles carrying large energies at both beam and target ver-

tices on the same events. As in Fig. 1, a dip at $n_{ch}=4$ may be attributed to the presence of events with no neutral particles, as demonstrated by the dashed points, where such events have been removed.

Comparing Figs. 2(b) and 2(c), we observe that the difference between $\langle \eta \rangle$ and $\frac{1}{2}\langle |x| \rangle$, arising from the track-by-track cancellations, is quite large at high n_{ch}. Further, even in the two-pronged events, with few neutral particles,[9] there are important cancellations among the neutral particles. The argument here is simple and illustrates these ideas. Thus,

$$\langle \eta^{\pm} \rangle_{2\,pr} \cong \tfrac{1}{2}\langle |x^{\pm}| \rangle_{2\,pr} ,$$

satisfying Eq. (5′), but

$$\langle \eta^{0} \rangle_{2\,pr} = 0.39 \pm 0.02$$

and

$$\tfrac{1}{2}\langle |x^{0}| \rangle_{2\,pr} = 0.29 \pm 0.01 ,$$

a clear disagreement. This disagreement is not due to the high-energy approximation used in Eq. (5′), because $\langle |x^0| \rangle$ is large; it must be due to cancellations among neutral particles of varying x on individual events. Hence, without having actually measured any of the neutral particles, we may conclude that emission of more than one neutral particle, into opposite c.m. hemispheres, is an important process in the two-pronged events.

In spite of the apparent simplicity of these quantities, the requirements of simultaneously accounting for Figs. 2(a)–2(c) forces strong quantitative constraints on relations among individual particle four-momenta which must be reproduced by serious models for high-energy processes.

In Fig. 2(c) we select the highest-rapidity negative and lowest-rapidity positive particles (note that because of the charge selections, these are not necessarily the highest- and lowest-rapidity particles) and plot their energy fractions separately. Although important in the c.m. momentum balance, these tracks do not play as substantial a role in the energy of the final state as might be supposed, as may be seen by comparing the data with the average energy per particle (curve labeled "equipartition," obtained assuming equal numbers of positive, negative, and neutral particles[9]). Only a few percent (less than 10% everywhere) of the total energy separates the average energies of these energetic tracks from those of the average tracks. We conclude that this provides little support for the designation of these particles as leading.

The inclusive average values of η are listed in Table II. We observe, as expected from Fig. 2(c), that the inclusive $\langle \eta^0 \rangle$ lies above $\langle \eta^+ \rangle$, which in turn lies above $\langle \eta^- \rangle$. We have not identified any experimental errors or effects that could explain these differences. In particular, the mass of the proton is not responsible for the $\langle \eta^+ \rangle - \langle \eta^- \rangle$ difference, since it has not produced a comparable difference between the η of the lowest-rapidity positive particles (expected to include most protons) and the highest-rapidity neagtive particles [Fig. 2(c)]. (If we use the lowest-p_{lab} positive track in place of the lowest-rapidity positive track, to test the effects of the mass dependence of rapidity, we arrive at the same conclusion.)

Finally, we note from Figs. 2(a)–2(c) that the behavior of the positive and negative systems is similar. The neutral particles show little or no overall preference (other than the slight negative value of $\langle x^0 \rangle$) to be produced more often in association with either the beam or the target. Therefore, the fact that beam and target contain different numbers and kinds of quarks has little effect on these variables. This is in spite of the fact that these variables are predominantly determined by the energy and momentum structure of the extreme regions, where one would expect to find fragments of the incident particles.

Laboratory energy fractions

The inclusive laboratory-frame energy fractions are also listed in Table II. These measurements are insensitive to the track mass, and therefore $\langle \eta_{lab} \rangle$ is very similar to $\langle p^c \rangle$ [Fig. 1(a)]. The changes in

TABLE II. Energy fractions.

	c.m. (η)	Laboratory
Sum of neutrals	0.374±0.006	0.34±0.01
Sum of positives	0.335±0.005	0.22±0.01
Sum of negatives	0.291±0.004	0.45±0.01

going from c.m. to laboratory are a reflection of the net motion of the particles in the c.m. [Fig. 2(a)]. We compare the results for the neutrals with a cosmic-ray experiment.

For this comparison we remove from $\langle \eta^c_{\rm lab} \rangle$ the estimated contribution of neutrons and neutral strange particles, totaling 5—10%, and obtain 0.31 ± 0.03 for the laboratory energy fraction for π^0 production. This we can compare with Azimov *et al.*[16] for the pionic component of the cosmic rays at 400 GeV average incident energy, whose results may extrapolated to proton targets to yield approximately 0.32—0.33, in good agreement.

Inelasticity

Inelasticity is a variable closely related to the energy fraction. It is the energy fraction of the nonleading particles. It is a familiar quantity in cosmic-ray data,[17,18] but very few results have been published from accelerator experiments, particularly at high energies. Inelasticity is an important variable in calculations describing the propagation of hadronic showers through the atmosphere[19] or other materials. Inelasticities much smaller than unity are usually taken as an indication that the interaction has a peripheral character.

Inelasticity may be measured for the event overall (K), at the target (K_T), or at the beam (K_B). In each case, we define K_j as the c.m. ratio of the appropriate incident energy (overall, at the target, or at the beam) minus the appropriate outgoing leading-particle energy, to the same incident energy minus the appropriate incident masses. For example,

$$K_T = (E_{\rm target} - E_{\rm leading\ out}) / (E_{\rm target} - m_{\rm target}) \ .$$

To calculate $E_{\rm leading\ out}$, we use the single extreme (in rapidity) charged particle in the appropriate direction. This single-leading-particle approximation to the leading particle causes K_j to be underestimated if the "true" leading particle has actually fragmented into more than one particle. However, it is a workable operational definition, and enables comparison with other results. To improve matters somewhat, we discard those events (with a compensating reweighting of the others) on which that chosen particle has the "wrong" charge. The "right" charge is negative if in the forward direction, positive if in the backward direction. If there is an identified proton on the event, it is used in calculating $E_{\rm leading\ out}$ for K and K_T, even in cases where it does not have lowest rapidity.

The results are shown in Fig. 3 as a function of $n_{\rm ch}$. Note that $\langle K \rangle$, which falls between $\langle K_B \rangle$ and $\langle K_T \rangle$, has been omitted from this figure for clarity.

We observe that $\langle K_B \rangle$ lies slightly below $\langle K_T \rangle$ in general, but that they agree almost everywhere within about 10%. As was the case earlier, the behavior of the beam vertex is similar to the target vertex over a wide range of inelasticity. Both $\langle K_B \rangle$ and $\langle K_T \rangle$ show behavior analogous to that seen for $\langle x \rangle$ [Fig. 2(a)], i.e., a rapid variation for low $n_{\rm ch}$, with a leveling off for $n_{\rm ch} \lesssim 10$ or 12.

When the data for K_T are restricted to those events with protons (corrected for those misidentified) the points labeled K'_T are obtained. We observe that, while $\langle K_T \rangle$ falls above $\langle K_B \rangle$, $\langle K'_T \rangle$ lies considerably below $\langle K_B \rangle$. Therefore protons are more energetic in the c.m. on the average than the lowest rapidity (i.e., the most energetic in the backward direction) π^+ on events with no proton. This is consistent with a model with a composite leading particle, in which a neutral baryon from its breakup receives more of its energy than any single meson, perhaps due just to mass effects.

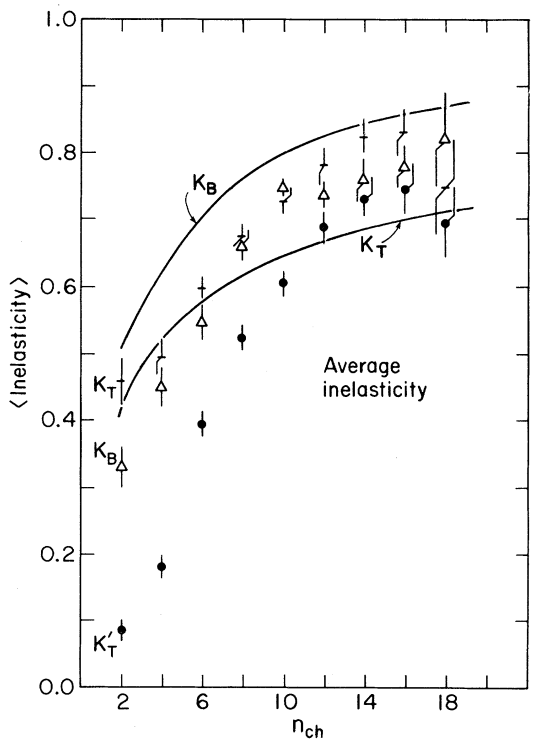

FIG. 3. Coefficient of inelasticity K (defined in text). At the target vertex (K_T); at the beam vertex (K_B); at the target vertex for events with protons (after correction for misidentified protons) (K'_T). Curves as in Fig. 2.

Behavior of the inclusive distributions

The inclusive K_T distribution is shown in Fig. 4; inclusive mean values of K, K_B, and K_T, and the corresponding primed quantities (events with protons only, corrected for those misidentified) appear in Table III. Shaded in Fig. 4 is K_T', which comprises 50% of the total area, by construction, due to the correction for misidentified protons (see the Appendix).

The contribution of events with scanner-identified protons is indicated by the dashed histogram. Note that such events are confined to small K_T, as expected (since identified protons have large $E_{\text{c.m.}}$), and that the correction provides a reasonable extrapolation from small to large K_T.

A strong peak is visible for $K_T \cong 0$, corresponding to beam diffraction dissociation.[8] The comparable structure expected for target dissociation at $K_B = 0$ (not shown) is not seen due to experimental resolution, a strong function of inelasticity, which at that point is ± 0.36 (based on elastic events). The data (and the misidentified proton correction) are uncertain near $K_T = 1$, and we can therefore draw no conclusions about this region.

Comparison with other experiments

An accelerator experiment[20] measuring inelasticity in pp collisions at 19 GeV/c, reports an average inelasticity of 0.54 (no error quoted). This result used identified final-state nucleons for the determination of E_N, hence, we compare with our primed quantities (Table III). For pp collsions, $\langle K' \rangle = \langle K_T' \rangle = \langle K_B' \rangle$; hence we should compare perhaps with our K_T' (Table III). We observe poor agreement. However, both experiments are subject to (different) systematic errors in proton identification. We observe good agreement with K'.

Cosmic-ray measurements of K', using primarily nucleon-nucleon collisions, find[17] average values

TABLE III. Inclusive inelasticity.

Quantity	Inclusive average
K	0.64 ± 0.01
K_B	0.61 ± 0.01
K_T	0.65 ± 0.01
K'	0.55 ± 0.01[a]
K_B'	0.62 ± 0.01
K_T'	0.46 ± 0.01[a]

[a]Statistical errors only.

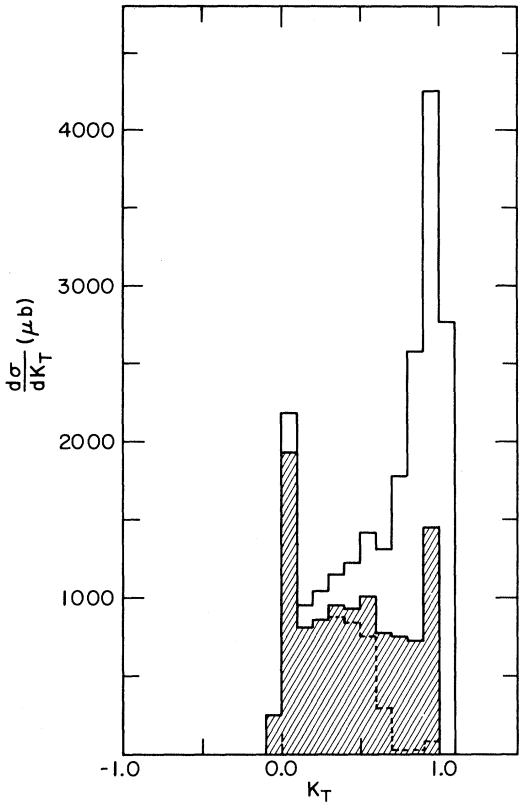

FIG. 4. Spectrum of target inelasticity K_T. Full histogram shows complete data; shaded are events with protons (after correction); dashed histogram: events with scanner-identified protons. Corrected proton events form a smooth continuation of identified proton events. The resolution, a strong function of inelasticity, is best near $K_T = 0$.

near 0.5, with a spread in values of about ± 0.15, nearly independent of energy from 25 to 3000 GeV. This is measured in the laboratory frame, with the leading particles identified as the fastest and slowest nucleons. Because the systematic errors, particularly in the identification of the leading particle and in the cosmic-ray primary energy determination, are large, we ignore the small correction required by the transformation from c.m. to laboratory frame.[18,21] The current results $\langle K' \rangle = 0.55 \pm 0.01$, $\langle K_T' \rangle = 0.46 \pm 0.01$ (Table III) are in the middle of the range of cosmic-ray data. Near our energy, a particular cosmic-ray experiment[22] which directly observed only the nonleading particles, reports $\langle K' \rangle = 0.37 \pm 0.02$, near the low range of cosmic-ray results. However, the quoted error includes no estimate of systematic errors.

We conclude that pion-proton and nucleon-

nucleon collisions show similar behavior in inelasticity over a wide range in energy, within the spread in experimental results.

Summary of Sec. III A

We have considered the behavior of a number of energy-momentum variables which are simple in conception, but which are of considerable value in analyzing the structure of the inelastic final states. In the laboratory frame, $p^{\pm,0}$ were shown, where the neutral particles are treated formally the same as the charged particles. We found that the negatives carry more momentum than the positives, on the average but that on $\sim 9\%$ of the events the positives, and on $\sim \frac{1}{3}$ of the events the neutrals, carry more than half the beam momentum. The extreme high and low values of $p^{\pm,0}$ are all dominated by low-multiplicity events. The high-multiplicity events have $p^{\pm,0}$ clustered around $\frac{1}{3}p_{\text{beam}}$ (although $\langle p^- \rangle > \langle p^+ \rangle$ for all topologies), with a relatively small fraction at very high or very low values.

We compared $\langle x \rangle$, $\langle |x| \rangle$, and $\langle \eta \rangle$ for all multiplicities. Some radical differences are seen, giving insight into the effects of both track-by-track cancellations in the sign of x_i and event-by-event cancellations in the sign of $\sum x_i$. A striking observation is that the resultant momentum of the sum of all neutral particles is approximately as large in absolute value as that of the positives or negatives, which are known to have large asymmetries arising from leading-particle effects. However, the small value of that resultant on the average over all events indicates that its sign must flip from event to event.

Inelasticity is widely used in cosmic-ray data analyses and in studies of the propagation of hadronic showers through matter. Our values agree with the main body of cosmic-ray data, showing inelasticity of both pion-nucleon and nucleon-nucleon collisions to be about one-half.

Most quantities we have shown display a strong n_{ch} dependence for $n_{\text{ch}} \lesssim 10$, and little dependence for $n_{\text{ch}} > 10$. A simple exchange model for the n_{ch} dependence we observe might require just two mechanisms, one of which (e.g., Pomeron exchange) is present only for low n_{ch}, with the proportion of events thus produced decreasing rapidly with rising n_{ch}, and completely gone by $n_{\text{ch}} \approx 10$. The signs we have seen for a flat n_{ch} dependence for $n_{\text{ch}} \lesssim 10$ would be readily accounted for in a model in which the dominant production mechanism is the same for the entire high-multiplicity region.[15] These points will be returned to in later discussion.

In general we may conclude that the quantities we have shown, which are sensitive to the extreme forward and backward kinematic regions, show no clear-cut dependence on the type of incident particle, i.e., in the backward hemisphere these variables are distributed in a way almost mirror symmetric to the forward hemisphere.

In the next section we examine the charge structure of the extreme forward and backward-regions in more detail.

B. Charge structure

In the preceding section, we studied the production characteristics of particles of different charge. In some cases the observed effects could be attributed to leading-particle production, since usually a net negative charge is associated with forward-going particles, and a net positive charge is associated with those going backward (in the c.m.).

In this section we study this question in more detail. The charge emission in the final state will be measured as a function of rapidity y. Other examples of studies of charge structure, of relevance to the present analysis, may be found in Ref. 11.

Rapidity-ordered charged preferences

We begin by listing the outgoing charged particles in an event in order of increasing rapidity. We then calculate the frequency f, averaged over all events, that the particle appearing at any particular location in the list is negative. The average charge $\langle q \rangle = 1 - 2f$. f will sometimes be given a superscript $(1, \ldots, n_{\text{ch}})$ and subscript (t or b) indicating the location relative either to the lower end of the list (near the target rapidity) or the upper end of the list (near the beam rapidity). For example, f_t^2 corresponds to the outgoing charged particle with the second lowest rapidity, and f_b^1 is the frequency with which the highest-rapidity charged particle is negative.

Purely random (e.g., thermodynamic) particle emission would predict $f_b^i = f_t^i = 0.5$. In the simple picture in which the highest-(or lowest) rapidity particle is a leading particle produced by neutral exchange (e.g., Pomeron), one expects $f_b^1 = 1.0$, $f_t^1 = 0.0$, and all the others to average 0.5. We will

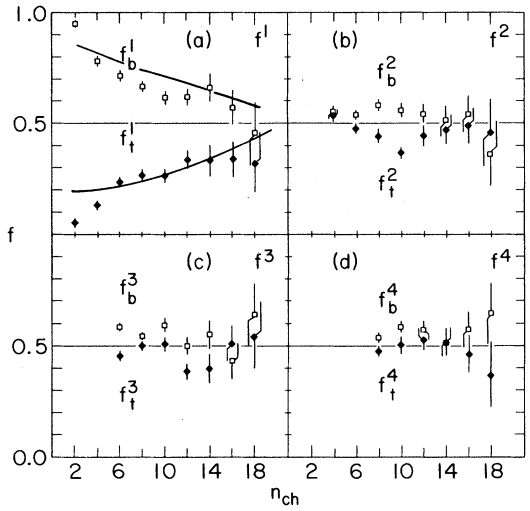

FIG. 5. n_{ch} dependence of average *negative* charge per event for specified particles ordered by rapidity. $f_b^n \equiv n$th outgoing particle in order from beam (highest-rapidity) vertex; $f_t^n \equiv$ same in order from target (lowest-rapidity) vertex. (a) $n=1$ ("extreme" particles) (b) $n=2$; (c) $n=3$; (d) $n=4$. For orientation, lines of no charge preference ($f=0.5$) are shown.

henceforth use the terminology "extreme particles" to denote these highest- and lowest-rapidity particles.

The data are shown in Figs. 5(a)—5(d), for $1 \leq n \leq 4$, as a function of n_{ch}. Redundant data points are eliminated; for example, for $n_{ch}=4$, $f_t^3=f_b^2$, and $f_b^3=f_t^2$, and are therefore deleted. For f_b^1 and f_t^1 we observe a rapid n_{ch} dependence at low n_{ch}, with approximate n_{ch} independence for $n_{ch} \gtrsim 10$. In that respect, this is similar to the behavior of $\langle p_{lab} \rangle$, $\langle x \rangle$, and $\langle |x| \rangle$ seen previously.

We further observe $f_b^1 > f_t^1$ for all n_{ch}. This supports the concept of leading particles, but since $f_b^1 \neq 1.0$ and $f_t^1 \neq 0.0$, the highest- (or lowest) rapidity charged particle actually has a charge *opposite* that of the beam (or target) a fraction of the time which is, for $n_{ch} \geq 10$, $\gtrsim \frac{1}{3}$. For example, for $n_{ch}=12$, $f_b^1=0.62\pm0.03$, indicating that although 62% of the extreme forward charged particles in this topology are negative, 38% of them are positive. Even for low multiplicities, e.g., $n_{ch}=4$, 21% are positive. We noted earlier the correlated result that in 9% of all events more than half the available momentum in the laboratory frame is carried by positive particles, and also that on 33% of the events at least half of the total momentum is carried by neutral particles. We conclude that in the forward direction, any leading-particle production which occurs is a complex process involving particles of all signs of charge, any one of which can under some circumstances carry a dominant fraction of the momentum of the leading particle. The same arguments may be applied also to the backward direction, because of the symmetry we have demonstrated.

In Figs. 5(b)—5(d) we observe that on average some "memory" of the incident charge is retained by outgoing particles at least up to the fourth removed from the extreme, i.e., there is a net charge preference. There is no apparent diminution in the size of the effect after the first. This means that incident-charge-related effects extend well away from the extreme outgoing particles.[23]

Inclusive values of $f_{b,t}^i$ are given in Table IV. From Table IV, it may be seen that $f_b^i \cong 1-f_t^i$, within a few percent, inclusively. From Fig. 5, the same results may be observed for each n_{ch}, within errors. Hence, we conclude there is a symmetry between processes at beam and target vertices in regard to average charge structure.

Rapidity size of charge-preference regions

We see from the above that the incident charge is reemitted over a range in rapidity, not concentrated in a single particle or at a single rapidity. With this in mind, we proceed to measure the average size of this range, in rapidity units.

We plot the rapidity y_i of particle i relative to the rapidity of the extreme particles. Define y_H as the highest charged rapidity actually observed on a given event, y_L as the lowest. Then we use the (non-negative) quantities $y_{Hi}=y_H-y_i$ and $y_{Li}=y_i-y_L$. One of the extreme particles therefore always lies at the origin; the abcissa measures rapidity distance from that point. In this experiment y_{Hi} and y_{Li} are ≤ 8 units. y_H, y_L, and y_H-y_L vary with the event.

In terms of these quantities we can study processes dependent upon rapidity distance from the extreme particles, rather than upon the absolute laboratory rapidity. If leading clusters, resonances, or fragmenting quarks are emitted, the charged particles from their decay will populate a certain range of rapidity. We should be able to measure the extent of this range in a manner insensitive to the actual rapidity at which the cluster or resonance is emitted if we look at f as a function of

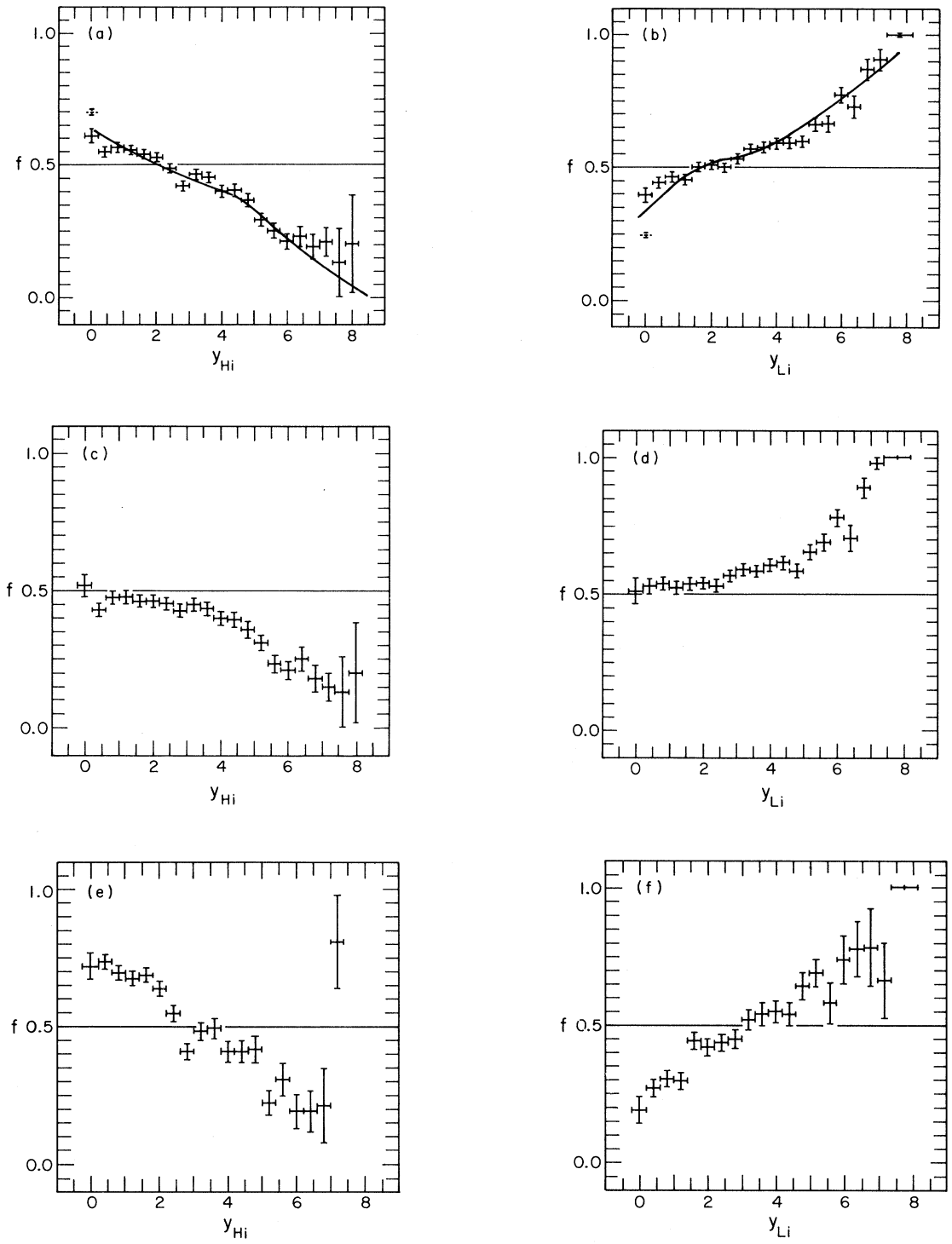

FIG. 6. Average *negative* charge per event as a function of rapidity relative to that of highest-y particle ($y_{Hi} \equiv y_{\text{highest}} - y_{\text{particle } i}$) or lowest-$y$ particle ($y_{Li} = y_{\text{lowest}} - y_i$). (a) As a function of y_{Hi}; (b) as a function of y_{Li}; (c) same as (a), requiring that particle H be negative; (d) same as (b), requiring particle L be positive; (e) complement to (c), i.e., requiring particle H be positive; (f) complement to (d), i.e., particle L is negative. The particles at $i = H$ or $i = L$ are shown dashed on parts (a) and (b) at 0.0; omitted otherwise. The maximum value of y_{Hi} or y_{Li} in this experiment is about 8 units.

y_{Hi} or y_{Li}. We shall see that we measure a larger size, or rapidity extent of the charge preference region, than other techniques have given for single cluster sizes, a fact which will be further discussed in Sec. IV.

We give f as a function of y_{Hi} in Fig. 6(a), and f as a function of y_{Li} in Fig. 6(b). The particles $i=H$ and $i=L$, appearing at $y_{Hi}=0$ and $y_{Li}=0$, respectively, are not included with the rest of the data, but appear as dashed points. Note that these points give the inclusive f_b^1 and f_t^1, respectively, also listed in Table IV. The lines of no charge preference, $f=0.5$, are shown on the figures, for reference.

On both Figs. 6(a) and 6(b), a clear structure may be seen. For low y_{Hi} (y_{Li}) the dominant charge is that of the beam (target). This dominance extends for a distance of about 2 units of rapidity in each case, followed by dominance of the opposite charge with little or no flat transition region in between. Each topology separately (not shown) shows similar structure. Hence, the incident charge prefers to be emitted locally, in rapidity, over a range of about 2 units at our energy. We will see below that this range does not contain a full unit of electric charge.

We can further investigate the question of charge structure by dividing the events into four categories; those that have a negative particle at $y_{Hi}=0$ and those that have a positive particle there and similarly at y_{Li}.

Figure 6(c) shows the resultant f as a function of y_{Hi} for events which have a negative particle at $y_{Hi}=0$ (the fixed-charge particle at $i=H$ is itself excluded from the figure). We observe a flat region extending about 3 units of rapidity from $y_{Hi}=0$, showing a slight preference for the charge opposite to that of the beam particle. Hence, in the region closely associated with the beam [which we shall define on the basis of Fig. 6(a) as $y_{Hi}\lesssim 2$] we observe a form of charge compensation: the charges emitted at these nearby rapidities partially cancel the beamlike charge of the extreme particle. Quantitatively, the average *total* charge emitted in $y_{Hi}\leq 2$ is $(-0.87\pm 0.03)e$ for these selected events; for the full data the result is $(-0.73\pm 0.02)e$. A similar (mirror image) effect is seen if Fig. 6(d), which shows f as a function of y_{Li} for events with the particle $i=L$ positive (that particle is again excluded from the figure). The average *total* charge in $y_{Li}\leq$ is $(+0.87\pm 0.03)e$ for these events; the full data gives $(+0.71\pm 0.02)e$. As a function of multiplicity (not shown) the average total charge emitted for $y_{Hi}\leq 2$ ($y_{Li}\leq 2$) is almost constant, becoming slightly more negative (positive) for $n_{\rm ch}=2$ and 4.

Corroborative results are seen in the behavior of the ordered charge frequencies f_b^n and f_t^n given inclusively in Table IV. Thus, if the highest-rapidity particle is negative (denoted by $f_b^1=1.0$), the particle next to it favors positive charge somewhat ($f_b^2=0.43\pm 0.02$). At the other extreme, we see a similar reversal of roles: given $f_t^1=0.0$, we find $f_t^2=0.55\pm 0.02$.

In Fig. 6(e), we now require the charge at $i=H$ be positive (that particle is excluded from the figure, as before). We observe a striking negative excess at low y_{Hi}; Fig. 6(f), where the charge at $i=L$ (excluded from the figure) is negative, shows a similar positive excess at low y_{Li}. This is a different manifestation of charge compensation, in which the compensation effect has more than canceled the charge of the extreme particle, but not enough so that a full unit of beamlike or targetlike charge is emitted in the beam-associated or target-associated regions. That is, the net charge for $y_{Hi}\leq 2$, including the positive particle at $i=H$, is $(-0.40\pm 0.05)e$, and for $y_{Li}\leq 2$, including the negative particle at $i=L$, is $(+0.23\pm 0.05)e$.

We conclude that there is a charge compensation effect in the extreme regions. Similar results are observed in e^+e^- collisions,[24] and other reactions.[12,25,26] We conclude further that less than one full unit of charge is emitted in any small rapidity interval including either extreme particle. In a multiperipheral-type model, this may be accomplished by "migration" of the incident charges toward each other in rapidity, leading to depletion of the net charge in the extreme region, or cancellation due to the presence of the opposite charge. In either case, with the opposite incident particles having opposite charge, neutral-leading systems may be produced.

We also observe "wrongly" charged leading systems: we find that for 10% of the cross section the net charge in $y_{Hi}\leq 2$ is positive, and symmetrically for $y_{Li}\leq 2$. It would be of interest to compare with π^+p reactions, for which migration of the incident charge *away* from the extreme region does not produce the same effect as migration of the opposite incident charge *into* the region.

In a simple quark model, if a clear leading jet is formed, it might have an average charge equal to that of the quark around which it formed: $\langle q\rangle_b=-\frac{1}{2}e$, $\langle q\rangle_t=\frac{1}{3}e$, the average beam and target valence quark charges. However, the data show $e>|\langle q\rangle|>\frac{2}{3}e$ in either $y_{Hi}\leq 2$ or $y_{Li}\leq 2$,

TABLE IV. Inclusive charge probabilities.

Specification[a]	Requirement[b]	Probability of negative charge
f_b^1		0.70±0.01
f_b^1	$f_t^1=0.0$[c]	0.71±0.01
f_b^1	$f_b^2=1.0$[d]	0.55±0.02
f_b^1	$f_b^2=0.0$[c]	0.87±0.01
f_t^1		0.24±0.01
f_t^1	$f_b^1=1.0$[d]	0.23±0.01
f_t^1	$f_t^2=0.0$[c]	0.40±0.02
f_t^1	$f_t^2=1.0$[d]	0.09±0.01
f_b^2		0.55±0.01
f_b^2	$f_b^1=1.0$[d]	0.43±0.02
f_b^2	$f_b^1=0.0$[c]	0.79±0.02
f_b^2	$f_t^1=0.0$[c]	0.58±0.02
f_b^2	$f_t^1=1.0$[d]	0.47±0.03
f_t^2		0.45±0.01
f_t^2	$f_b^1=1.0$[d]	0.41±0.02
f_t^2	$f_b^1=0.0$[c]	0.55±0.02
f_t^2	$f_t^1=0.0$[c]	0.55±0.02
f_t^2	$f_t^1=1.0$[d]	0.19±0.02
f_b^3		0.55±0.01
f_t^3		0.47±0.01
f_b^4		0.55±0.02
f_t^4		0.49±0.02

[a]For f^2, exclude $n_{ch}=2$; for f^3, exclude $n_{ch}=2$, 4; for f^4, exclude $n_{ch}=2$, 4, 6.
[b]Blank indicates no requirement imposed.
[c]Specified particle is positive.
[d]Specified particle is negative.

and in all smaller regions including the extreme particles. We find this to be only weakly dependent upon y_H or y_L (actually showing a slight increase as the rapidity separation y_H-y_L of the extreme particles, which might be a measure of the "clearness" of the leading jet, increases). Thus we have no evidence for clear leading single-quark jets.

Finally, careful comparison of Figs. 6(c) and 6(e), which display disjoint samples of events, indicates that they are nevertheless in close agreement with each other in the high-y_{Hi} region (greater than about 2 or 3 units). A similar comparison of the data of Figs. 6(d) and 6(f) leads to the same conclusion, for y_{Li}, although in this case close agreement is seen only for $y_{Li}\gtrsim 4$ or 5 units. We conclude that the average charge structure at sufficiently great rapidity distances from a given extreme particle is completely independent of the charge on that particle.

The idea that the behavior of the target vertex is independent, up to kinematic factors, of the behavior of the beam vertex is known as factorization. By a study of the charge structure as in Fig. 6 we are able to test this idea in a single sample of events, rather than, for example, by comparing target dissociation for different beam particles. We find consistency, for rapidity regions sufficiently far separated.

The inclusive rapidity-ordered frequencies f_b^1 and f_t^1 support this finding (Table IV). That is, f_b^1 is unchanged, within errors, by the requirement $f_t^1=0.0$, and f_t^1 is likewise independent of f_b^1. However, the nearest-neighbor (second-highest and lowest-rapidity) particles do not share this property: f_b^2 is correlated with f_t^1, and f_t^2 is correlated with f_b^1.

Total rapidity span

In Fig. 7 we display the mean total rapidity span of the charged secondaries, $\Delta y_{tot}=y_H-y_L$. This falls in the rather narrow range of about 4–5 units, decreasing only slowly with n_{ch}. The charged particles become increasingly densely populated in rapidity as n_{ch} increases. The inclusive average is 4.79±0.03 units. Therefore, the size of one of the

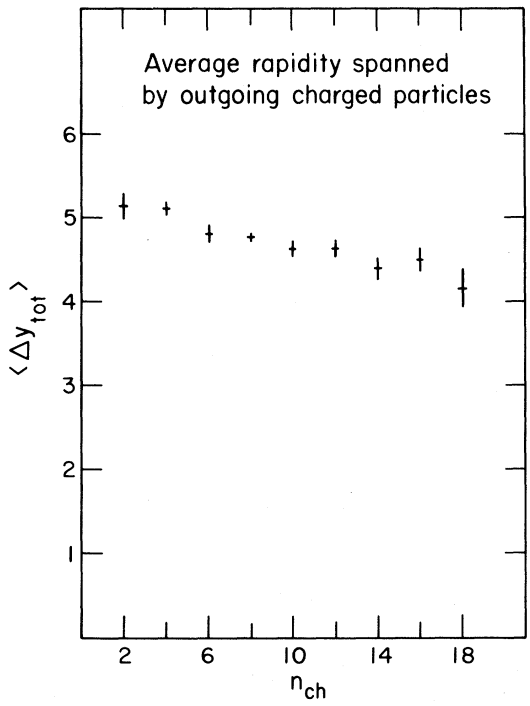

FIG. 7. The average total range of rapidity, Δy_{tot} spanned by all charged particles, as a function of n_{ch}.

regions of charge dominance established above, 2—3 units, covers just about half of the average total rapidity range populated by the charged secondaries.

Hence, on the average event the two opposite rapidity regions dominated by the charges of the incident particles must meet. This suggests that the lack of a central region of no charge preference arises because these regions terminate only by encountering the region of opposite sign. The results of an experiment with a neutral target, Kladnitskaya *et al.*,[11] support arguments that the regions throughout which the charges of the incident particles are reemitted are even larger than the 2—3 units of rapidity inferred from Figs. 6(a) and 6(b). We have similarly discussed evidence [e.g., Figs. 6(c) and 6(d)] that the rapidity region populated by the particles that are carrying off the net target charge actually overlaps with that of the beam charge, and vice versa. Since the extreme particles are independent of each other, we can set an upper limit to the size of these regions as less than $\langle \Delta y_{\text{tot}} \rangle$. Experiments at very great energy are necessary to see if these regions separate and leave a true central region in between.

Finally, we find (not shown) that the region of charge preference is not confined to large absolute rapidities (near the beam or target). A slight average charge preference is suggested even for particles with very small c.m. longitudinal momenta.

Effect of Δ^{++} production

Strong Δ^{++} production, visible[27] at least up to $n_{\text{ch}}=10$, is an obvious mechanism for generating charge structure differences between beam and target fragmentation regions. The absence of a known $\pi^-\pi^-$ resonance precludes an analogous effect at the beam vertex, and non-doubly-charged resonances occur at both beam and target vertices, where they may be expected to have similar effects. However, comparison of Figs. 6(c) and 6(d) shows no significantly greater tendency for positives at low y_{Li} to lie close together than for negatives at low y_{Hi}. Further, f_t^2 [Fig. 5(b)] shows no dip at low n_{ch}, where Δ^{++} production has the largest fraction of the topological cross section. There is a suggestion of a dip for $n_{\text{ch}}=10$, which might be attributed to nondiffractive Δ^{++} production. However, for the same n_{ch}, we find $f_t^2=0.61\pm0.04$ (i.e., to favor negative charges) when it is required that the lowest-rapidity particle be positive ($f_t^1=0.0$), approximately mirror symmetric with the result at the beam vertex: $f_b^2=0.45\pm0.05$ when $f_b^1=1.0$, contrary to expectations for any strong Δ^{++} influence.

We conclude that no clear charge-correlation effects due to Δ^{++} production are visible in these distributions.

Summary of Sec. III B

We have studied the charge structure of the emitted particles in order to clarify the role of the charge incident at each vertex. We find that the extreme particles carry that charge off more than $\frac{2}{3}$ of the time overall, but that this fraction varies from about 95% for the two-pronged events down to 50 or 60% for the highest multiplicities studied. The second-, third-, and fourth-highest- (and lowest-) rapidity charged particles show a definite net preference for the charge of the incident beam (target) particles also, a preference which is approximately independent of charged multiplicity. These particles are far more likely to carry this charge when the extreme particle itself has the opposite charge.

As a function of rapidity distance from the extreme particles, we observe a preference for the incident charge which decreases smoothly until, after

about 2 or 3 units, the preference changes sign, with no appreciable transition region. We define this distance to be the size of the region closely associated with the incident particle. When events are selected with the extreme particle having a given charge, the nearby particles exhibit a compensation effect. This has the result that the net charge emitted in the region closely associated with a given incident particle is less than a full unit of charge, but greater nevertheless than the average charge of the quarks in the incident hadrons.

The charge structures in rapidity regions separated by a sufficiently large interval (at least ~ 4 units) are independent of each other, consistent with factorization. In particular, the average charges of the opposing extreme particles are independent of each other.

We have further shown that the average "span" of the events is just about double the span of either of the charge-preference regions. Hence, we infer that the two opposite-charge-preference regions are juxtaposed. In fact, they might have extended for more than 2 or 3 units of rapidity in the absence of the cancellation from the opposing charge from the other extreme.

We find that these results are not sensitive to the actual c.m. rapidity at which the extreme particles are emitted. Finally, we observe no noticable influence of the doubly charged Δ^{++} resonance on this charge structure.

IV. COMPARISON WITH A SIMPLE CLUSTER MODEL

These data provide a basis for testing models of inelastic hadronic reactions. Models which describe the process in terms of the emission of a limited number of groups of particles, clusters, or jets, have received a great deal of attention.[28] Clusters which may be thought of as generalized resonances, provide a framework for the description of such effects as short-range order. If produced by a multiperipheral type of mechanism, clusters exhibit strong momentum-transfer, and, hence, transverse-momentum damping, and are emitted at irregular intervals of rapidity as illustrated in Fig. 8. Leading clusters are shown with solid lines; an example of overlap of two clusters is explicitly shown.

We performed a calculation of a specific model to simulate the present experiment, based on an extension of a suggestion of Chan *et al.*[29,30] Briefly, we have considered production of two or more clusters with mass spectrum given by the model. Cluster decay multiplicities and particle charge assignments are chosen by us as a function of cluster mass to resemble real resonances. Charge 0, ± 1 exchange is allowed; a second version of the model, allowing only zero charge exchange, was also computed and will be occasionally referred to for comparison. Baryon exchange is neglected. We have adjusted no parameters to fit the data. The mean total number of particles turns out to be $\langle n_{\text{tot}} \rangle = 11.7$ with an rms width of 4.6 and $\langle n_{\text{ch}} \rangle = 8.0$ with an rms width of 3.1, compared with the actual data, which have $\langle n_{\text{ch}} \rangle = 7.99 \pm 0.06$ with an rms width of 3.87 for the inelastic channels.[9] The model incorporates a single trajectory for all exchange links. Hence, we expect variables dependent upon momentum-transfers to agree with the data only on the average over all exchanges (including Pomeron). The number of π^0's per event is roughly equal to $n_{\text{ch}}/2$ as in the real data,[9] although it is somewhat higher at low n_{ch}.

The results may be seen as hand-smoothed curves in Figs. 2, 3, 5, and 6.

Nonzero $\langle x^{\pm} \rangle$ [Fig. 2(a)] comes from forward-backward c.m. asymmetries occurring in charged particle production. In cluster models, such asymmetries can arise as a consequence of "limited leading charge flow." That is, the average charge of the clusters produced nearest the beam in rapidity is expected to be negative, and those nearest the target positive (we neglect double charge-exchange throughout). This occurs because the charge which is incident at opposite ends of the rapidity axis (Fig. 8) must be either exchanged or emitted at each successive cluster emission point. Therefore, even if one adopts a model in which charge exchange is somewhat favored over neutral exchange,

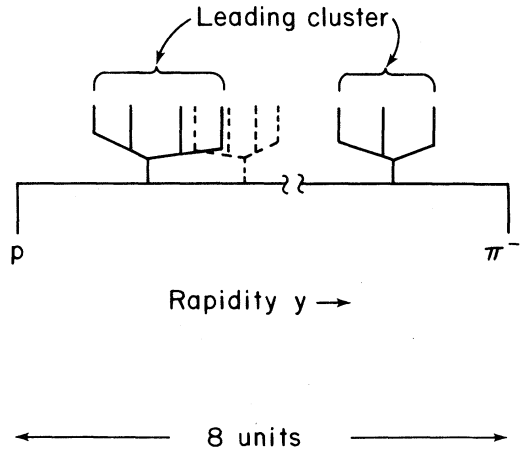

FIG. 8. Rapidity-axis diagram illustrating emission of clusters.

the "flow" of incident charges toward each other down the rapidity axis will be interrupted by emission at some point, or by mutual annihilation. Clearly, any cluster emitted at higher y than the negative cluster of largest y must have net charge zero, and similarly at the other extreme.[28]

We can understand qualitatively some features of the behavior of $\langle x^{\pm} \rangle$ [Fig. 2(a)] if we make the simplifying assumption of no charge flow. That is, the highest-y cluster is negative, the lowest-y one is positive, and all others are neutral. Then, assuming forward-backward symmetry in the production of all clusters other than the leading ones, $\langle x^{\pm} \rangle$ is determined by the leading clusters, being a function of their average momentum transfer and mass. For fixed mass, increasing momentum transfer reduces the longitudinal momentum of leading clusters and hence brings $\langle x^{\pm} \rangle$ closer to zero. If the average mass of the leading cluster is at most a weak function of $n_{\rm ch}$, then the argument may be reversed to show that $\langle x^{\pm} \rangle$ provides a measure of this average momentum transfer, which is a function of the exchange mechanism. In most models, only a finite set of such mechanisms is expected to contribute significantly. Therefore there should exist a maximum value to the average momentum transfer we expect to observe. We call this effect "limiting peripherality," since a maximum to the average momentum transfer implies a certain lower limit to the character of the interactions known as "peripherality."

Experimentally, we have noted a tendency for $\langle x^{\pm} \rangle$ to flatten out at small magnitudes at high $n_{\rm ch}$ [Fig. 2(a)]. Similar tendencies appear also in $\langle p^{\pm} \rangle$ [Fig. 1(a)], $\langle |x^{\pm 0}| \rangle$ [Fig. 2(b)], and possibly also $\langle K_T \rangle$ and $\langle K_B \rangle$ (Fig. 3). This behavior is consistent with limiting peripherality, because a plausible interpretation of the leveling off is that it is a result of saturation of the momentum transfer to the leading clusters. That is, at high multiplicities the (allowed) exchange which produces the maximum average momentum transfer is dominant.

In the model calculation, we find $\langle x^{\pm} \rangle$ roughly constant [Fig. 2(a)], which is to be expected by this reasoning, because only a single type of exchange is used for all $n_{\rm ch}$. We find also, by comparison with the calculation with no charge exchange, that $\langle x^{\pm} \rangle$ is not sensitive to the amount of charge exchange called for in the model. Hence, the assumption of zero charge exchange made previously may be relaxed.

We have found, by varying the proportion of π^0's in the model, that $\langle \eta^0 \rangle$ is sensitive to the proportion of neutral pions per event. Thus, the rise in $\langle \eta^0 \rangle$ seen at low $n_{\rm ch}$ for the model reflects the predicted increase in the proportion of π^0's to charged particles at low $n_{\rm ch}$.

In Figs. 6(a) and 6(b) the charge-exchange model (shown) is in good agreement with data. The model without charge exchange (not shown) is in reasonable (but not quite as good) agreement; the contribution of charge exchange to the observed size of the regions of charge dominance (~ 2 units) is not clearly established by these calculations. In both versions of the model, the rapidity region populated by the charged decay products of a single cluster is only about 0.5 to 0.6 units wide on the average (dominated by single-charged-particle clusters of zero width), in reasonable agreement with the estimate from correlation studies, ~ 0.7 units,[11] but the distribution of these cluster widths extends beyond 2 units. In the absence of charge exchange, the presence of regions of charge dominance extending beyond ~ 0.6 units can be explained as being due to unusually broad leading clusters carrying the charge of the beam or target.

In conclusion, we have calculated a cluster model for comparison with the data. Serious discrepancies are observed with the distributions of energy and momentum variables, although averages over all $n_{\rm ch}$ are in fair agreement. It is likely that there would be better agreement between model and data if a more complete set of exchange mechanisms were incorporated.

V. SUMMARY

We have shown distributions of novel variables which are simple conceptually, and easy to calculate, and which provide new insight into 205 GeV/c $\pi^- p$ interactions. The results provide constraints on models for multiparticle production. Our results are most sensitive to processes occurring at the opposing extreme regions of the rapidity spectrum.

The charged-summed variables p^c, x^c, and η^c allow us to treat all charges $c = +, -, 0$ on an approximately equal footing. Taking averages over numerous events reduces the effect of random experimental errors. The results show clear asymmetries for all topologies. In the c.m. the negatives have net momentum forward, the positives backward. The neutrals turn out to be as asymmetric as the charged particles, but the sign of the asymmetry varies from event-to-event, leaving only slight net backward motion on the average over all

events. The negative-positive asymmetry decreases with n_{ch} until approximately $n_{ch}=10$, beyond which a saturation effect appears to be present. This saturation effect, which we call "limiting peripherality," could be attributable to the dominance at high n_{ch} of a single exchange mechanism. Indeed, a model calculation incorporating a single exchange mechanism for all topologies shows a nearly flat n_{ch} dependence.

These asymmetries find a natural explanantion in terms of leading-particle production with limited leading charge flow. That is, the leading particles (which may also be clusters, resonances, or jets, and which can be defined in a multiperipheral picture as those particles emitted at one of the extreme vertices of the multiperipheral diagram) may either carry the charge incident at the vertex or be neutral, so that the average is not neutral. This behavior has been shown not to be confined to diffractive processes, as defined herein.

The beam and target vertices show similar behavior in all variables studied. No statistically significant effects traceable to Δ^{++} (1238) or other resonance production have affected this similarity. The independence of the two vertices (or their "factorizability") has been tested with respect to the charge structure of the opposite extreme regions and found to hold for events with sufficiently great rapidity span.

The c.m. energies are partitioned nearly equally among the charges, with the positives receiving about $\frac{1}{3}$ of the energy, the neutrals somewhat more, the negatives somewhat less. These fractions are roughly topology-independent. In the laboratory, the negatives get nearly $\frac{1}{2}$ the energy, the neutrals $\frac{1}{3}$, the positives the remainder, on the average over all events. As a function of topology, both negatives and positives show a strong variation in $\eta^{\pm}_{lab}$ [which is approximately proportional to $p^{\pm}$, Fig. 1(a)], in contrast with the c.m. case.

The single highest- or lowest-rapidity charged particles cannot be uniquely identified as the leading particles. For example, in $\sim 30\%$ of the cases, they have a charge opposite to that of the incident particle. In cluster models, this is at least partly a consequence of overlap of the decay products of nearby clusters, as illustrated in Fig. 8. However, we have also seen that in many events most of the laboratory energy is possessed by neutral or positive particles. Thus beam-associated leading particles have a significant probability of transferring most of their energy to particles of nonbeamlike charge. These phenomena find a natural explanation if leading clusters decay into several particles, some of which are neutral or positive. Then there must be a substantial probability that most of the laboratory energy of the cluster appears on a single particle, which may be any one of the decay products. The large number of events with high-energy neutral particles suggests that the number of neutral decay products of forward leading clusters may be comparable to the number of negative decay products, on the average.

The insight we gain into leading-particle behavior with the use of the above variables does not depend on requiring any particular rapidity gap between particles, such as is often needed when an attempt is made to separate and identify leading particles. Indeed, we have shown that the regions of charge preference are contiguous in rapidity with no evidence for a featureless central region, making such a separation at best an ambiguous process.

We have measured inelasticity for events in which the incident charge is carried by the highest- or lowest-rapidity charged particle or by a proton, in the hope of thereby determining a significant fraction of the energy of the leading particle. This provides a useful comparison with cosmic-ray results available over an enormous energy range, from which we deduce that the extreme regions are similar in πp and pp collisions from 25 to 3000 GeV, consistent with limiting fragmentation. The target inelasticity computed from the outgoing nucleon appears considerably different from the beam inelasticity computed from an outgoing π^-, but this may be a consequence of neglect of other particles produced in beam and target fragmentation rather than a real difference between the vertices. The n_{ch} behavior of the inelasticity suggests again that a change in the dominant production mechanism occurs around $n_{ch}=10$, with little or no n_{ch} dependence thereafter.

The distribution of leading charge has been studied by looking at charge imbalances as a function of rapidity distance from the leading (outgoing) edge of the event, in two ways. First, we looked at the first, second, etc., particles in order of rapidity from the leading edge, otherwise ignoring the rapidity at which they were emitted. We find that the first particle has a strong charge bias which depends on multiplicity. Also, the second and subsequent particles retain some memory of the charge of the corresponding incident particle.

Second, we studied the size of the rapidity region over which charge dominance was observed,

measured with respect to the extreme particles. This size, about 2 units, is about half the average total rapidity spread populated by the charged secondaries, and is not very sensitive to the actual rapidity at which the particles are emitted. This size is larger than the average rapidity spread of charged particles from clusters, estimated from correlation studies to be ~ 0.7 units.[11] From our calculations, which predict the average rapidity spread of clusters to be $0.5-0.6$, in reasonable agreement with that number, it appears that the 2-unit size we observe can be explained as a consequence of leading clusters with greater than average rapidity spread, possibly accompanied by leading charge flow. There is evidence to suggest further that the characteristic y range populated by particles which carry off the beam or target charge might be larger than 2 units. That is, in some events the leading charge in the first 2 units of rapidity may be partly or wholly canceled by "flow" of the leading charge out of the region or of the opposite leading charge into the same region. For example, the net charge excess in the 2 units of rapidity over which dominance is observed is less than one full unit of charge (in absolute value). As an extreme case, on about 10% of the events a net charge opposite to that of the nearby incident particle is emitted in the first 2 units of rapidity.

If leading charge flow occurs, then neutral leading clusters are produced. Some evidence for this comes from the existence of events with large missing momentum in the laboratory; neutral leading clusters decaying entirely into neutrals (e.g., $n\pi^0$) would produce such events.

The cluster-model calculation we have presented represents a worthwhile first step in understanding these events, but cannot be taken too seriously in view of its disagreement with aspects of the data. The logical next step would appear to be to incorporate a realistic set of exchange mechanisms to replace the single effective trajectory we have used. Reproducing the distributions we have presented provides, we believe, an effective yet simple test of the ability of any model to describe high-energy $\pi^- p$ interactions.

ACKNOWLEDGMENTS

We thank the accelerator, beam, and bubble-chamber staffs at Fermilab, and the film-analysis staffs at all laboratories participating. We wish to express our appreciation to G. S. Abrams, C. Gee, C. Friedberg, G. Goldhaber, F. R. Huson, D. Ljung, S. Pruss, and G. H. Trilling for their contributions to earlier phases of the experiment. Useful discussions with F. Henyey and J. Dash are gratefully acknowledged. This work resulted from Fermilab experiment E137, and was supported in part by the U. S. Department of Energy, the National Science Foundation, and the French Centre National de la Recherche Scientifique.

APPENDIX: TRACK MISIDENTIFICATION

All tracks other than identified protons are taken to be pions. This identification was subjected to verification at the analysis stage, based on a comparison between the reconstructed π^+ and proton interpretations of the track, using (i) the calculated projected ionization and (ii) the value of the mass-dependent rms deviations on film of the measured points from the fitted curve (FRMS). With the use of these criteria, the identification of a track was changed from proton to π^+ or vice versa on about 5% of the events. From study of events having four-constraint (4C) fits, where the protons are identified kinematically, the efficiency of the final-proton identification was found to be nearly 100% for proton momenta below 400 MeV/c, decreasing to about 70% at 1.1 GeV/c, and falling rapidly for higher momenta. The average for all 4C inelastic fits (predominantly four- and six-pronged events) is 88%.

Misidentification of a track does not significantly affect its laboratory momentum determination. However, the track mass assignments may have important effects in the transformation to the c.m. system. Because most variables used in this analysis involve groups of particles rather than single tracks, the effects of mass misidentification of a single track are diluted. The most important effects are due to misidentified protons. $K^\pm$ and $e^\pm$ tracks occur less often than protons and do not differ in mass from the pion as much as protons, hence their effects are estimated to be smaller. Further, they should affect positives and negatives approximately equally, and therefore are not likely to seriously affect comparisons between positives and negatives.

On the basis of charge independence one might expect the baryon to emerge as a neutron on roughly $\frac{1}{2}$ the events.[31] The observed fraction of the events with an identified proton is a smoothly

decreasing function of n_{ch}, from $\sim 50\%$ for $n_{ch}=2$ (inelastic) to about $10-20\%$ for $n_{ch}>10$, a fact we attribute to misidentification of protons. Corrections for this effect were estimated on the basis of a subsample of the events on which tracks duplicating the probable characteristics of misidentified protons were found. These tracks, at most one per event, were assigned a proton mass, and events thus doctored were included with an appropriate weight (described below) in the "identified proton" sample.

The proton-simulating tracks were selected from events with no identified proton. The positive track with the largest production angle on a random side of the event with respect to the beam, as viewed in projection, was chosen. Events in which the selected track had momentum less than 1.0 GeV/c were then discarded, since we believe that $> 70\%$ of such real protons have been identified, and these tracks do not therefore reflect the true characteristics of misidentified protons.

By selecting on the basis of production angle rather than momentum we have some protection against underestimation of high-momentum protons. That is, we do not always select the slowest track on the event. On the other hand, on the high-multiplicity events, for which the greatest correction is made, the sheer number of positive tracks provides protection against overestimation of the number of fast protons.

We chose weighting factors for these simulated-proton events such that the total of events with identified plus simulated protons represented 50% of each topological cross section, separately.[31] Events without identified protons are correspondingly weighted to represent the remaining 50%. Note that some events are included in both samples.

The final correction is negligible in most distributions for low n_{ch}, becoming comparable to one standard deviation only for $n_{ch}=14$ and higher, in most cases. The inelasticity (and, hence, c.m. energy) of simulated protons forms a smooth continuation of the distribution obtained with identified protons (Fig. 4), indicating that the correction is reasonable.

---

*On leave from Université Paris VI, Paris, France.
†Present address: Laboratoire de l'Accelerateur Lineaire, Orsay, France.
‡Present address: Dalmo-Victor Company, Bell-Aerospace, Belmont, California.
§Present address: Fermi National Accelerator Laboratory, Batavia, Illinois.
||Present address: Washington University, St. Louis, Missouri 63110.
¶Present address: Brookhaven National Laboratory, Upton, L.I., New York.

[1]See, for example, J. Whitmore *et al.*, Phys. Rev. D 16, 3137 (1977), for $\pi^{\pm}$ at 100 GeV/c.
[2]W. B. Fretter *et al.*, Phys. Lett. 57B, 197 (1975) (a preliminary version of this paper was submitted to the 1975 APS Conference in Seattle, Washington).
[3]L. Stutte, thesis, University of California, Berkeley, 1974 (unpublished).
[4]W. R. Graves, thesis, University of California, Berkeley, 1977 (unpublished).
[5]D. M. Chew *et al.*, Report No. LBL-2106, 1973 (unpublished).
[6]D. Bogert *et al.*, Phys. Rev. Lett. 31, 1271 (1973); F. C. Winkelmann *et al.*, Phys. Lett. 56B, 101 (1975).
[7]H. H. Bingham *et al.*, Phys. Lett. 51B, 397 (1974).
[8]F. C. Winkelmann *et al.*, Phys. Rev. Lett. 32, 121 (1974); F. C. Winkelmann *et al.*, in *Particles and Fields—1973,* proceedings of the Berkeley Meeting of the Division of Particles and Fields of the American Physical Society edited by H. H. Bingham, M. Davier, and G. Lynch (AIP, New York, 1973), p. 359.
[9]D. Ljung *et al.*, Phys. Rev. D 15, 3163 (1977). Similar results at 250 GeV/c were obtained by R. N. Diamond *et al.*, *ibid.* 25, 41 (1982).
[10]Three View Geometry Program, F. Solmitz *et al.*, Alvarez Group Programming Note No. p-117 (unpublished); SQUAW, O. I. Dahl *et al.*, Alvarez Group Programming Vote No. p-126 (unpublished).
[11]See, for example, V. P. Kenney *et al.*, submitted to the Meeting of the Division of Particles and Fields of the APS, Seattle, 1975 (unpublished); see also J. W. Lamsa *et al.*, Nucl. Phys. B135, 258 (1978); Phys. Rev. Lett. 37, 73 (1976); M. Della Negra *et al.*, Phys. Lett. 59B, 401 (1975); J. Whitmore, in *Particles and Fields 76,* proceedings of the Annual Meeting of the Division of Particles and Fields of the APS, edited by H. Gordon and R. F. Peierls (BNL, Upton, New York, 1977). A relevant analysis at 40 GeV/c has been reported by E. N. Kladnitskaya *et al.*, Yad. Fiz. 23, 809 (1976) [Sov. J. Nucl. Phys. 23, 426 (1976)]. Interesting results at lower energy have been reported by C. V. Cautis *et al.*, submitted to the Meeting of the Division of Particles and Fields of the APS, Seattle, 1975 (unpublished); P. Lauscher *et al.*, Nucl. Phys. B106, 31 (1976).
[12]A review of these points is given by M. LeBellac, in Report No. CERN 76-14, 1976 (unpublished).
[13]This variable is also discussed by D. Sivers, in *The Strong Interactions,* proceedings of the SLAC Summer Institute on Particle Physics, 1974, edited by M.

C. Zipf (SLAC, Stanford, 1974), Vol. 1, p. 327.

[14]We select diffractive events as follows: (i) for beam dissociation, the mass-squared recoiling against an identified proton is required to be less than 30 GeV^2, as in Ref. 8; (ii) for target dissociation, we require each of the following: (a) the resultant momentum of the system of charged particles recoiling against the fastest π^- be <25 GeV/c, (b) the total mass-squared of that system be <30 GeV^2, (c) the angle of the fastest π^- with respect to the beam be <0.01 rad, after an adjustment for possible momentum mismeasurement. This adjustment consists of setting the absolute value of the momentum of the fastest π^- to the maximum value consistent with longitudinal momentum conservation, and then using the known correlation between measured momentum (i.e., curvature) and measured production angle to adjust the angle.

[15]In a two-component model involving diffractive production (fraction f_D of the channel) plus other (fraction $f_{\rm ND}=1-f_{\rm D}$), the value of, say, $\langle x^-\rangle$ is given by $\langle x^-_{\rm diff}\rangle f_D+\langle x^-_{\rm nondiff}\rangle f_{\rm ND}$, where $\langle x^-_{\rm nondiff}\rangle$ would be estimated by $\langle x^-_{n^-_{\rm ch}>10}\rangle\cong 0.2$. Then, for a given $n_{\rm ch}$,

$$f_D=\frac{\langle x^-\rangle-\langle x^-_{\rm nondiff}\rangle}{\langle x^-_{\rm diff}\rangle-\langle x^-_{\rm nondiff}\rangle}\ .$$

With the ansatz $\langle x^-_{\rm diff}\rangle=1$, we find that this value of f_D is in reasonable agreement with the results of Ref. 8, topology by topology. See also the encircled points, Fig. 2(a).

[16]S. A. Azimov *et al.*, Izv. Akad. Nauk. SSSR, Ser. Fiz. 38, 898 (1974).

[17]A review of cosmic-ray work has been given by E. L. Feinberg, Phys. Rep. 5, 237 (1972).

[18]L. F. Hansen and W. B. Fretter, Phys. Rev. 118, 812 (1960).

[19]For example, T. K. Gaisser, J. Geophys. Res. 79, 2281 (1974); T. K. Gaisser, R. H. Maurer, and C. J. Noble, in *Proceedings of the Thirteenth International Conference on Cosmic Rays, Denver, 1973* (Colorado Association University Press, Boulder, 1973), Vol. 4, p. 2652; T. K. Gaisser and G. B. Yodh, *ibid,* Vol. 3, p. 2140.

[20]H. Boeggild *et al.*, Nucl. Phys. B91, 365 (1975).

[21]A. Sh. Gaitinov, Zh. S. Takibaev, and I. Ya Chasnikov, Izv. Akad. Nauk. SSSR, Ser. Fiz. 35, 2083 (1971).

[22]These results were presented in Ref. 17 based on work described in N. A. Dobrotin and S. A. Slavatinsky, *Tenth International Conference on Cosmic Rays, Calgary, Alberta, Canada, 1967,* edited by R. J. Prescott (University of Calgary, Alberta, Canada, 1967), Part A, p. 416; N. A. Dobrotin *et al.*, Can. J. Phys. 46, 5675 (1968).

[23]This point will be discussed additionally later. It does not depend on the second or subsequent particles carrying large momenta [refer to the triangular points, Fig. 2(a)]. In this comparison, we implicitly neglect the difference between selection of the extreme track on the basis of Feynman x, as in Fig. 2(a), and on the basis of rapidity, as in Fig. 5, which we find experimentally to be small.

[24]G. G. Hanson, in *Weak Interactions—Present and Future,* proceedings of SLAC Summer Institute on Particle Physics, 1978, edited by M. C. Zipf (SLAC, Stanford, 1978).

[25]See, for example, the review of K. Zalewski, in *Proceedings of the XVII International Conference on High Energy Physics, London, 1974,* edited by J. R. Smith (Rutherford Laboratory, Chilton, Didcot, Berkshire, England, 1974), p. I-93.

[26]See, for example, the review of W. Ko, in *Proceedings of the XVII International Conference on High Energy Physics, London, 1974* (Ref. 25), p. I-76. For π^-p at 205 GeV/c, see Biswas *et al.*, Phys. Rev. Lett. 35, 1059 (1975).

[27]H. H. Bingham *et al.*, Report No. LBL-3855, 1975 (unpublished); N. N. Biswas *et al.*, Phys. Rev. D 16, 2090 (1977); D. Brick *et al., ibid.* 18, 3099 (1978).

[28]See, for example, D. Brick *et al.*, Phys. Rev. D 24, 590 (1981) for an analysis of π^-p at 147 GeV/c; other work is summarized in Ref. 12.

[29]Chan. H. M. *et al.*, Nucl. Phys. B92, 13 (1975).

[30]A. Gula, in *High Energies and Elementary Particles,* proceedings of the International Symposium, Warsaw, 1975 (Joint Institute for Nuclear Research, Dubna, 1975), p. 108.

[31]The assumption that for each topology separately the fraction of events with protons is equal to 0.5 is consistent with the 100 GeV/c results of J. E. A. Lys *et al.*, Phys. Rev. D 16, 3127 (1977), who find that the fraction of the time that a struck proton yields a proton or a YK^+ pair ($Y\equiv$ hyperon) rather than a neutron or a YK^0 pair is 0.61 ± 0.08 overall, with little or no topology dependence. The probability of YK^+ is not known, but a feeling for the importance of hyperon production may be obtained from the known (Ref. 9) fraction of inelastic events with a Λ^0: 0.08 ± 0.02 in this experiment. Therefore all YK^+ probably comprises several percent of the cross section and hence, 0.5 is seen to be a reasonable estimate of the fraction of inelastic events with a proton.